

Acoustic radiation from vortex-barrier interaction in atomic Bose-Einstein condensate

K. Suthar, Arko Roy, and D. Angom

Physical Research Laboratory, Ahmedabad - 380009, Gujarat, India

(Dated: May 26, 2022)

We examine the dynamics of a vortex dipole in the Bose-Einstein condensates (BECs) of trapped dilute atomic gases at zero temperature in the presence of a Gaussian barrier potential. The density-anisotropy induced by the barrier enhances the acoustic radiation from the vortex dipole. This is due to the deviation of the condensate density from the equipotential curves and variation in the curvature of the vortex dipole trajectory. Due to the acoustic radiation, the vortex dipole dissipates energy and spirals towards the edge of the condensate. As a result, we observe an increase in the vortex-antivortex annihilation events. To examine the effect of the Gaussian barrier, we estimate the correction to the Thomas-Fermi condensate density using perturbation expansion method and the results are in very good agreement with the numerical results.

PACS numbers: 03.75.Lm, 03.75.Kk, 67.85.De

I. INTRODUCTION

The dynamics of topological defects like vortex in non-linear systems is the key to understand important phenomena in chemical patterns, fluid dynamics, liquid crystals, superfluids, etc [1–3]. In scalar Bose-Einstein condensates (BECs) [4–6], vortices carry integral angular momentum and serve as the obvious signature of superfluidity of these systems [7, 8]. The various experimental techniques which have been employed to generate vortices in BECs include manipulating the interconversion between the internal spin states of an isotope [9], stirring the BEC with a laser beam [10], rotating the BEC [11], phase imprinting [12–14] and merging of BECs [15]. Vortex dipoles, consisting of vortex-antivortex pairs, have also been experimentally realized in BECs by moving the condensate across a Gaussian obstacle potential [16]. In a vortex dipole, vortices of opposite circulation cancel each other's angular momentum and thus carry only linear momentum. This is the cause of several fascinating phenomena such as leap frogging, snake instability [17], etc. Another important dynamical phenomenon is the vortex-antivortex annihilation, which is expected to occur when vortex and antivortex approach each other. There is, however, a dearth of experimental signature. The introduction of a Gaussian barrier, examined in the present work, ensures the vortex-antivortex annihilation occurs by modifying the trajectories through acoustic radiation by the (anti)vortex.

On the theoretical front, among other important phenomena, creation and dynamics of a vortex dipole in a BEC at zero temperature [18–20], lack of annihilation of vortex dipoles [21, 22], effect of an oscillating Gaussian potential [23], and impact of the density inhomogeneity on the vortex motion [24] have been examined in previous works. The stability and dynamics of the clusters of vortices and antivortices in pancake-shaped BECs has also been studied [25]. It may also be mentioned here that in phase-separated binary condensates, coreless vortex dipoles can be formed by passing an obstacle across the condensate [26] or changing the nonlinearities associated

with the system [27]. The dynamics of a vortex dipole across an interface of quasi-2D two-component BEC has also been examined in Ref. [28].

Despite these significant experimental and theoretical advances, the interactions between a single vortex or a vortex dipole with a barrier (which can be experimentally achieved through a laser beam), within a BEC, and the associated vortex dynamics, are not fully understood and many problems remain unexplored. At zero temperature, in the absence of any other dissipative mechanism, the acceleration of a vortex generates acoustic radiation, which is the only sink of the turbulent kinetic energy [29, 30]. The decay of a single vortex, due to inhomogeneity induced acoustic emission in a combined harmonic and Gaussian dimple trap potential has been studied in a previous work [31]. Similar studies have also examined the acoustic radiation from multiple vortices of same circulation or charge in a harmonic [32] and double-well [33] trapping potentials.

In the present work, we investigate theoretically the interaction of a vortex dipole in a harmonically trapped quasi-2D BEC with a repulsive Gaussian barrier using the Gross-Pitaevskii equation (GPE). The presence of the barrier breaks the rotational symmetry of the system and introduces novel effects on the dynamics of the vortex dipole. As a result of broken rotational symmetry, the equipotential and the isodensity curves do not coincide, hence the vortex or antivortex which precess along the equipotential curves traverse regions of different densities. When the vortex dipole encounters the barrier region, it emits acoustic radiation and some part of the kinetic energy is dissipated. This leads to a change in the trajectories of the vortex-antivortex pair which gradually spirals out of the condensate. The study of vortex dipole interaction with a barrier in a BEC will shed light on the process of dissipation of kinetic energy into acoustic energy, and as well as the conditions for annihilation along with other phenomena arising from the dynamics of vortex dipoles.

The paper is organized as follows. In Section II we describe the dynamics of vortex dipole using matched

asymptotic expansion technique. In the same section we also discuss the correction to Thomas-Fermi(TF)-approximation near the Gaussian barrier, and examine the curvature and tidal effects. The Section III is concerned with the numerical study of the dynamics of vortex dipole in the presence of the barrier in quasi-2D trap and the power radiated near the barrier. We, then, end with conclusions in Section IV.

II. BEC WITH VORTICES

In the mean-field approximation, the time dependent GPE describes the dynamics of a weakly interacting BEC of dilute atomic gases very well. This implies $an^{1/3} \ll 1$ where, a and n are the s -wave scattering length of the atoms and density of the BEC, respectively. Thus, the order parameter of a single species scalar condensate, Ψ , is given by the GPE

$$i\hbar \frac{\partial}{\partial t} \Psi(\mathbf{r}, t) = \left[-\frac{\hbar^2}{2m} \nabla^2 + V_{\text{ext}}(\mathbf{r}) + U|\Psi(\mathbf{r}, t)|^2 \right] \Psi(\mathbf{r}, t), \quad (1)$$

where V_{ext} is an external trapping potential, and $U = 4\pi\hbar^2 a/m$ is the strength of inter-atomic interaction with m as the atomic mass. The order parameter Ψ is normalized to the total number of atoms N in the condensate. For the present study, V_{ext} consists of a harmonic confining potential V_{tr} and a repulsive Gaussian barrier potential along the x -axis V_{bar} , which passes through the origin,

$$\begin{aligned} V_{\text{ext}}(\mathbf{r}) &= V_{\text{tr}} + V_{\text{bar}}, \\ &= \frac{m\omega_{\perp}^2}{2}(x^2 + y^2 + \alpha^2 z^2) + V_0 \exp\left(-2\frac{y^2}{w^2}\right) \end{aligned} \quad (2)$$

where ω_{\perp} is the radial trapping frequency, α is the anisotropy parameter (ω_z/ω_{\perp}), and V_0 and w are the amplitude and width of the Gaussian barrier, respectively. For the present work, N is sufficiently large so that $\mu \gg \hbar\omega_{\perp}, \hbar\omega_z$ and TF approximation is applicable in the bulk of the condensate. In this approximation, the order parameter is $\Psi_{\text{TF}} = [(\mu - V_{\text{tr}})/U]^{1/2}$. However, this approximation does not provide a good description in the regions where the condensate density has large gradients, and the kinetic energy is not negligible. We consider quasi-2D geometry (pancake shaped) of the trapping potential, which implies $\alpha \gg 1$ or $\omega_z \gg \omega_{\perp}$.

A. Dynamics of vortices in BEC

The hydrodynamic equations corresponding to the GPE represents an irrotational flow. Vortices, however, may occur when there are phase singularities in Ψ . The motion of a vortex line in the condensate depends on the trapping potential, angular velocity of the trap and distortion of the vortex line. The expression for the vortex

velocity has been calculated using coordinate transformations and the method of matched asymptotic expansion [34–36], where the TF approximation is used in the matching region. A vortex element carrying charge q located at the position \mathbf{r}_0 from the center of a rotating trap with angular velocity $\mathbf{\Omega}$, has velocity [37]

$$\begin{aligned} \mathbf{v}(\mathbf{r}_0) &= \frac{\hbar q(\hat{z} \times \hat{t})(\partial V_{\text{tr}}/\partial z)|_{\mathbf{r}=\mathbf{r}_0}}{2mU|\Psi_{\text{TF}}|^2} [\ln(\xi) + \hat{\rho} \otimes \hat{\rho}] \\ &+ \frac{\hbar q \kappa \hat{b}}{2m} \left[\ln\left(\frac{1}{\xi} \sqrt{\frac{-\rho_0}{\kappa \hat{b} \cdot \hat{\phi}}}\right) + \hat{\rho} \otimes \hat{\rho} \right] \\ &+ \frac{\hbar q[\hat{z} \times \nabla V_{\text{tr}}(\mathbf{r}_0)]}{2mU|\Psi_{\text{TF}}|^2} \left[\frac{3}{2} \ln\left(\frac{R_{\perp}}{\xi}\right) + \hat{\rho} \otimes \hat{\rho} \right] \\ &+ 2 \frac{\nabla V_{\text{tr}}(\mathbf{r}_0) \times \mathbf{\Omega}}{\nabla_{\perp}^2 V_{\text{tr}}(\mathbf{r}_0)}, \end{aligned} \quad (3)$$

where \hat{t} , \hat{n} and \hat{b} are the tangent, normal and binormal vectors, collectively form the Frenet-Serret coordinate system. These are orthogonal vectors which form a basis of the local coordinate system centered at the vortex element. Any point on the vortex line at a radial distance ρ_0 from the trap center is represented by (ρ, ϕ, z) in cylindrical coordinates. The unit vectors $\hat{\rho} \approx \mathbf{r}/\rho$ and $\hat{\phi}$ are along radial and azimuthal directions, defined for the far-field region with respect to the vortex element. The parameter R_{\perp} is the radial extent of Ψ_{TF} , κ is the curvature of the vortex line, and $\xi = \hbar/\sqrt{2mnU}$ is the healing length, where $n = |\Psi_{\text{TF}}|^2$ is the local density of the condensate. The parameter ξ is an important quantity as it is a measure of the vortex core size. Here, the symbol \otimes represents the tensor product of two radial unit vectors.

In the present work, we consider a quasi-2D nonrotating trapped condensate for which $\mathbf{\Omega} = 0$. We can also assume $\kappa \approx 0$, since the curvature of the vortex lines do not play any significant role in a quasi-2D system. Thus the dynamics of a vortex dipole in quasi-2D condensate is solely governed by the third term of Eq. (3). Based on which, a single off-axis vortex moves along an equipotential curve and the vortex precess around the trap center. In the case of multiple vortices in the condensate, the inter-vortex induced velocity must also be included. Here, we consider the case of a vortex-antivortex pair or a vortex dipole, with the vortex and antivortex located at \mathbf{r}_1 and \mathbf{r}_2 , respectively. Thus, the velocity component of the vortex due to the presence of the antivortex is given by

$$\begin{aligned} \mathbf{v}_{12} &= -q \frac{\hbar}{m} \nabla \phi_2(\mathbf{r}_1), \\ &= q^2 \frac{\hbar}{m} \frac{[\nabla \times (|\Psi_{\text{TF}}|^2 \Phi(\mathbf{r}_1, \mathbf{r}_2) \hat{z}_1)]}{|\Psi_{\text{TF}}|^2}, \end{aligned} \quad (4)$$

where ϕ_2 is the phase of the condensate associated with the antivortex. In above equation we can write $\nabla \phi_2$ at the location of vortex as $-q[\nabla \times (|\Psi_{\text{TF}}|^2 \Phi(\mathbf{r}_1, \mathbf{r}_2) \hat{z}_1)]/|\Psi_{\text{TF}}|^2$, with \hat{z}_1 being the unit vector in the vortex's frame. This form is chosen such that

it satisfies the property $\nabla \cdot (|\Psi_{\text{TF}}|^2 \nabla \phi_2) = 0$ [37]. The *pseudo-vector potential* in the above equation is defined as

$$\Phi(\mathbf{r}_1, \mathbf{r}_2) = -K_0 \left(\sqrt{\frac{\nabla_{\perp}^2 V_{\text{tr}}}{2U|\Psi_{\text{TF}}|^2}} |\mathbf{r}_1 - \mathbf{r}_2| \right), \quad (5)$$

where K_0 is the modified Bessel function of the second kind.

During the dynamical evolution, the vortex and antivortex are closest when they traverse the bulk of the condensate where TF-approximation is applicable. Within the bulk of the condensate, $\nabla_{\perp}^2 V_{\text{tr}} / (2U|\Psi_{\text{TF}}|^2) \approx 1/R_{\perp}^2$. For small separation between vortex and antivortex,

$$\Phi(\mathbf{r}_1, \mathbf{r}_2) \approx \ln \left(\frac{e^{\gamma} |\mathbf{r}_1 - \mathbf{r}_2|}{2R_{\perp}} \right), \quad (6)$$

where we have used $K_0(x) \approx -\ln(e^{\gamma}x/2)$ for $x \rightarrow 0$ [38] and γ is the Euler constant.

The trajectory of a vortex dipole results from the competition between the effects of vortex-antivortex interaction and precession [39]. The net velocity of the vortex or antivortex is the sum of the individual velocity, third term of Eq. (3), and the mutual velocity field given by Eq. (4). In the calculation of the individual velocity, we neglect $\hat{\rho} \otimes \hat{\rho}$ as it is smaller than the logarithmic term [37]. Additionally, the contribution from mutual velocity field is dominant when the vortex-antivortex pair is closely separated. This happens in the bulk-region of the condensate where $|\Psi_{\text{TF}}|^2$ is assumed to be constant. Thus, the dynamics of a vortex dipole consisting of a singly charged vortex ($q = 1$) and antivortex ($q = -1$) located at (x_1, y_1) and (x_2, y_2) , respectively, is given by the following coupled differential equations.

$$\begin{aligned} \mathbf{v}_i = & (-1)^{i+1} \frac{3\hbar[\hat{z}_i \times \nabla_i V_{\text{tr}}(\mathbf{r}_i)]}{4mU|\Psi_{\text{TF}}|^2} \ln \left(\frac{R_{\perp}}{\xi} \right) \\ & + \frac{\hbar}{m} \left[\nabla_i \times \ln \left(\frac{e^{\gamma} |\mathbf{r}_i - \mathbf{r}_j|}{2R_{\perp}} \right) \right] \hat{z}_i, \end{aligned} \quad (7)$$

where $i = 1$ and 2 represents the vortex and antivortex, respectively, and $j = 3 - i$. After simplification, we get

$$\begin{aligned} \mathbf{v}_i = & (-1)^i \frac{3\hbar\omega_{\perp}^2}{4U|\Psi_{\text{TF}}|^2} (y_i \hat{x}_i - x_i \hat{y}_i) \ln \left(\frac{R_{\perp}}{\xi} \right) \\ & + \frac{\hbar}{m} \left[\frac{(y_i - y_j) \hat{x}_i - (x_i - x_j) \hat{y}_i}{|\mathbf{r}_i - \mathbf{r}_j|^2} \right], \end{aligned} \quad (8)$$

where the unit vectors \hat{x}_i , \hat{y}_i and \hat{z}_i are defined along the local coordinates of the vortex and antivortex.

Now, we consider the effect of the Gaussian barrier potential on the dynamics of the vortex dipole. Since we introduce the barrier along x -axis, it affects the x component of the velocities when $|y_i| \leq w$, while the y component of the velocities remain unaffected. This is because from Eq. (7), using V_{ext} in place of V_{tr} , the velocity of the vortex or antivortex depends on $(-1)^{i+1} \hat{z}_i \times \nabla V_{\text{ext}}(\mathbf{r}_i) \approx$

$(-1)^{i+1} \hat{z}_i \times (\partial V_{\text{bar}} / \partial y_i) \hat{y}_i$. The vortices cross the barrier two times in an orbit, which is evident from the trajectories shown in Fig. 1(b). The first and second crossings occur when vortex-antivortex are far and closely separated, respectively. The effect of the barrier potential is more prominent in the former as the intervortex interaction is negligible. In this case within the barrier region ($|y_i| \leq w$) and neglecting intervortex interaction, the velocities along the x -axis are

$$\mathbf{v}_{ix} = (-1)^i \frac{3\hbar\omega_{\perp}^2}{4U|\Psi_{\text{TF}}|^2} \left(1 - \frac{4V_0}{m\omega_{\perp}^2 w^2} \right) y_i \ln \left(\frac{R_{\perp}}{\xi} \right) \hat{x}_i, \quad (9)$$

where we have retained only the first term in the expansion of V_{bar} . Away from the barrier ($|y_i| > w$), the influence of the barrier potential is weak and may be neglected. The modified velocities, thus, depend on the barrier parameters V_0 and w . We choose V_0 sufficiently large ($V_0 \gg m\omega_{\perp}^2 w^2$) such that it affects the dynamics of the vortices in the quasi-2D BEC and in particular, the velocity component along x -direction.

B. Correction to TF approximation

The presence of the barrier along x -direction in the condensate introduces a large density gradient in y -direction. Thus, for $|y_i| \leq w$ the TF approach fails to describe the system and this motivate us to calculate the deviation from TF approximation. The leading order correction to the TF approximation may be calculated using standard perturbation expansion techniques [40–42]. In the present work we examine the correction to the TF density profile along y -direction due to the presence of the Gaussian barrier using an approach similar to ref. [40].

To describe the structure of Ψ near the repulsive barrier, we consider the condensate in the quasi-2D limit ($\alpha \gg 1$). In this regime, we approximate the equilibrium order parameter as $\Psi(x, y, z, t) = \exp(-i\mu t/\hbar) \psi(x, y) \phi_0(z)$, where $\phi_0(z) = [\alpha/2\pi]^{1/4} \exp(-\alpha z^2/4)$ is the ground state wave function along the z -direction and μ is the chemical potential. Using this ansatz in Eq. (1) and integrating over z -direction, we obtain the dimensionless 2D GPE

$$\begin{aligned} & \left[-\frac{1}{2} \left(\frac{\partial^2}{\partial \tilde{x}^2} + \frac{\partial^2}{\partial \tilde{y}^2} \right) + \frac{1}{2} (\tilde{x}^2 + \tilde{y}^2) + \tilde{V}_0 \exp \left(-2 \frac{\tilde{y}^2}{\tilde{w}^2} \right) \right. \\ & \left. + \tilde{g} |\tilde{\psi}(\tilde{x}, \tilde{y})|^2 \right] \tilde{\psi}(\tilde{x}, \tilde{y}) = \tilde{\mu} \tilde{\psi}(\tilde{x}, \tilde{y}), \end{aligned} \quad (10)$$

where we use the oscillator length $a_{\text{osc}} = \sqrt{\hbar/(m\omega_{\perp})}$, ω_{\perp}^{-1} , and the oscillator energy $\hbar\omega_{\perp}$ as the dimensional units of length, time and energy, respectively. The effective dimensionless 2D interaction strength $\tilde{g} = 2\sqrt{\pi}\alpha(a/a_{\text{osc}})$. Here, $\tilde{\mu}$ is the shifted chemical potential in scaled units obtained after integrating out the axial

direction z from the GPE in 3D. For notational simplicity, we will represent the scaled quantities without tilde in the rest of the manuscript.

Without the barrier potential the equipotential curves coincide with the isodensity curves and a single vortex (antivortex) precess along these curves in anticlockwise (clockwise) direction. As the barrier potential is along x -axis, and $V_0/w^2 \gg 1$, for $|y|/w \ll 1$ we have $\partial V_{\text{ext}}/\partial x \ll \partial V_{\text{ext}}/\partial y$. So, in this region we can consider $\nabla_{\perp} V_{\text{ext}} \approx \hat{y} \partial V_{\text{ext}}/\partial y$ with \hat{y} defined as the unit vector along the y -direction and the vortices undergo a large change in velocity. The Eq. (9) shows that, the velocity of the vortex and antivortex is dependent on the y -coordinate within the barrier region. When the vortex or antivortex enters the barrier region, it experiences a sharp deceleration for $y \sim w$ but the velocity drops to zero at $y = 0$ and again for $y \sim -w$, it experiences an acceleration till it leaves the barrier region. This is confirmed with numerical computations for the antivortex velocity.

To estimate the leading order correction to ψ_{TF} , we consider the case of $V_0 = \mu$, so that ψ_{TF} is zero at the origin. This assumption simplifies the calculation of the correction in the condensate order parameter near the barrier. Thus, for $|y|/w \ll 1$ with the above considerations at a fixed value of x , Eq. (10) simplifies to

$$\left[-\frac{1}{2} \frac{\partial^2}{\partial y^2} + \frac{1}{2} y^2 + V_0 \exp\left(-2\frac{y^2}{w^2}\right) + 2a\sqrt{\pi\alpha} |\psi(y)|^2 \right] \psi(y) = \mu \psi(y), \quad (11)$$

where we have redefined μ by subsuming the x component of the trapping potential. We introduce a scaled length variable $\zeta = y/\delta$, where δ is the distance between the center of the trap and classical turning points (where total energy is equal to the potential energy) near the barrier in y -direction. In the $|y| < \delta$ region the kinetic energy is not negligible and this is the prime reason for calculating the correction to TF-approximation. In this regard, δ is a characteristic length which is associated with the structure of the barrier and number of atoms in the system. The scaled variable is such that $\delta \ll 1$ and $\zeta \gg 1$, but $\delta\zeta \ll w$. In this domain, the barrier potential $V_0 \exp(-2y^2/w^2) \approx V_0(1 - 2\delta^2\zeta^2/w^2)$ and Eq. (11) becomes

$$-\psi'' - \mu' \psi + \eta \zeta^2 \psi + \nu \psi^3 = 0, \quad (12)$$

where the prime denotes the differentiation with respect to the scaled variable ζ , $\mu' = 2(\mu - V_0)\delta^2$, $\eta = (1 - 4V_0/w^2)\delta^4$ and $\nu = 4a\delta^2\sqrt{\pi\alpha}$. Thus the solution with the TF-approximation is

$$\psi_{\text{TF}} = \left(\frac{\mu' - \eta \zeta^2}{\nu} \right)^{1/2} \text{ for } \zeta \gg 1. \quad (13)$$

To determine the leading order correction to ψ_{TF} , we define $\psi = \psi_{\text{TF}} + \psi_1$ and treat ψ_1 as a correction arising

from the presence of the barrier along x -direction. After linearizing Eq. (12) and only considering terms linear in ψ_1 , we get

$$-\psi_1'' - (\mu' - \eta \zeta^2) \psi_1 + 3\nu \psi_{\text{TF}}^2 \psi_1 = \psi_{\text{TF}}''. \quad (14)$$

Now, after neglecting ψ_1'' , as it contributes to terms of higher order in $1/\zeta^2$, the correction ψ_1 is

$$\psi_1 = \frac{-\eta \mu'}{2\nu^{1/2} (\mu' - \eta \zeta^2)^{5/2}}. \quad (15)$$

Thus, the corrected solution of the GPE in Eq. (11) with the TF-approximation is

$$\psi = \left(\frac{\mu' - \eta \zeta^2}{\nu} \right)^{1/2} \left[1 - \frac{\eta \mu'}{2(\mu' - \eta \zeta^2)^3} \right]. \quad (16)$$

With this improved solution, the equipotential and isodensity curves do not coincide anymore and as a consequence, the vortex or antivortex which precess along the equipotential curves traverse regions of different densities. Due to the density inhomogeneity, the vortex or the antivortex experiences a change in the velocity and generates acoustic radiation. In other words, there is a change in the kinetic energy of the vortex or antivortex as a part of it is transformed into acoustic radiation energy.

C. Curvature and tidal effects

In addition to the change in velocity arising from the density gradient, the vortex or antivortex also undergoes acceleration due to the curvature of the equipotential curves of V_{ext} . With only the harmonic oscillator potential, the equipotential curves are circles and have constant curvature. However, in the presence of the barrier potential, the equation of equipotential curve with energy C in 2D is

$$\frac{1}{2}(x^2 + y^2) + V_0 \exp\left(-2\frac{y^2}{w^2}\right) = C, \quad (17)$$

where $C \leq R_{\perp}^2/2$. The equation of the curve can be rewritten as a function of y and we can then calculate the curvature at a point on the curve. From basic differential geometry, for any two points with the same abscissa x , and $\pm y$ as the y -coordinate on an equipotential curve, the curvature is given by

$$K = \left| \frac{d\varphi}{ds} \right| = \left[2C - 2V_0 \exp\left(-2\frac{y^2}{w^2}\right) \right]^{-1/2}, \quad (18)$$

where φ and s are the angle subtended by the tangent to the x -axis and arc length of the curve. This indicates that for $|y| \ll w$ we get $K \approx (2C + 4V_0 y^2/w^2 - 2V_0)^{-1/2}$, which can be large when $|y|/w \sim 1$. So, when the vortex or antivortex traverses this region it undergoes large acceleration and induces acoustic radiation. In the region where $|y| > w$ the effect of barrier is negligible and

$K \approx 1/\sqrt{2C}$. Due to the constant K , as mentioned earlier, the vortex or antivortex undergoes uniform acceleration and generates acoustic radiation [31]. However, the power radiated is much smaller than in the region with large changes in K . Later, we shall examine the temporal variation of the radiated energy J in detail with numerical simulations.

To illustrate the dissipation process, we consider the case of a single vortex passing through the barrier potential. The velocity of vortex near the barrier can be understood in terms of the vortex velocity field given in the Eq. (9). According to the equivalence between a 2D superfluid and (2+1)D electrodynamic system, the vortices, superfluid density, and particle current play the roles of charges, magnetic field and electric field, respectively. Most importantly, the acoustic waves in the superfluid are analogous to the electromagnetic radiations [43]. The acoustic radiation from the vortex, due to large K , near the barrier is similar to the Larmor radiation from an accelerating charged particle [44]. The energy radiated in the far field is

$$J = \lim_{r \rightarrow \infty} \int_0^{2\pi} \mathbf{S} \cdot \hat{n} r d\theta, \quad (19)$$

where the Poynting vector in the leading order is $\mathbf{S} = (\partial\phi/\partial t)\nabla\phi$ [45] with ϕ as the phase of the condensate, $r = \sqrt{x^2 + y^2}$ is the circle enclosing the vortex and \hat{n} is the normal to the circle at a point. We analyze the radiation in the regions far from the location of the vortex and antivortex. This is done by using far-field approximation, where the radiation emitted are similar to the acoustic waves [46]. In the far-field limit $\nabla\phi \cdot \hat{n} \approx \dot{\phi}/c$, where $c = \sqrt{|\psi|^2 g}$ is the acoustic speed and thus, the power radiated depends on the temporal variation of ϕ . To examine the temporal variation of ϕ , we resort to the hydrodynamic description of the condensate. This is equivalent to the inviscid hydrodynamic equations with an additional term to represent the quantum pressure. The latter, quantum pressure, is important at the length scales of ξ or smaller and for the system of current interest $\xi \sim 0.2 - 0.4\mu m$. This range of ξ is derived from the density in the bulk region through the relation $\xi = 1/\sqrt{2|\psi|^2 g}$, where we use ψ obtained from the numerical solution of the GPE.

Since the barrier potential is along x -axis, we can neglect the density variation along x -axis in comparison to the y -direction. For a fixed value of x we can write $\psi(y, t)|_x = \sqrt{n(y, t)/n} \exp[i\phi(y, t)]$, with n as the average condensate density. The dimensionless GPE can then be recast as two coupled equations of n (in y -direction) and ϕ as,

$$\dot{n} = -\partial_y [n\partial_y\phi], \quad (20a)$$

$$\dot{\phi} = -\left[V_{\text{ext}} + ng - \frac{1}{2} \frac{\partial_y^2 \sqrt{n}}{\sqrt{n}} + \frac{1}{2} (\partial_y\phi)^2 \right]. \quad (20b)$$

In the second equation, the term with \sqrt{n} arises from the quantum pressure. The other effect of the barrier arises from the large $\partial V_{\text{ext}}/\partial y$ when $|y| \leq w$. Due to this large gradient, two points within the vortex core separated by $\Delta y \ll 1$ have large difference in velocity. This distorts the geometry of the vortex core from circle to ellipse as it enters the domain of the barrier potential. The velocity difference between two points of the vortex separated by 2ξ along y -axis, based on the first term in Eq. (7), is

$$\begin{aligned} \Delta v &= v(x, y - \xi) - v(x, y + \xi) \\ &= \frac{3}{2}\xi^2 \left[\hat{z} \times \left(\nabla V_{\text{ext}}(x, y - \xi) - \nabla V_{\text{ext}}(x, y + \xi) \right) \right] \ln \left(\frac{R_{\perp}}{\xi} \right), \end{aligned}$$

and finally using the scaled expression for the V_{ext} , we get

$$\begin{aligned} \Delta v &= \frac{3\xi^3}{w^4} \left[\exp \left(\frac{2y^2 + 2\xi^2}{w^2} \right) (w^4 - 16y^2\xi^2) - 4(w^2 - 4y^2)V_0 \right] \exp \left(\frac{-2y^2 - 2\xi^2}{w^2} \right) \ln \left(\frac{R_{\perp}}{\xi} \right). \quad (21) \end{aligned}$$

This finite difference in velocity across the vortex core near the barrier gives rise to tidal effect. Furthermore, the core also acquires higher multipole moments due to the deviation from circular geometry. The shape of the core is well described by the ratio n_v/n_0 , where n_v and n_0 denotes the density of the condensate with and without vortex, respectively [47]. It must be mentioned that, the vortex precession velocity depends on the background velocity field evaluated around the core and the shape of the vortex core [48]. So, the barrier height and distortion of the core due to the tidal effect have direct bearing on the vortex dynamics. We shall examine it in more detail with the numerical computations.

III. NUMERICAL RESULTS

In the numerical simulation, we solve the dimensionless GPE using the Crank-Nicholson method [49] with following set of parameters: we consider ^{87}Rb atoms with $a = 99a_0$ (where a_0 is the Bohr radius), $N = 1 \times 10^5$, $\alpha = 25$ and $\omega_{\perp} = 2\pi \times 10\text{Hz}$. We use phase numerical implementation of the imprinting method [50] to generate vortex dipole in BEC. For this, we begin the simulation with imaginary time propagation of the GPE and imprint the phase corresponding to a vortex dipole by using

$$\begin{aligned} \psi(x, y) &= |\psi(x, y)| \exp \left[iq \tan^{-1} \left(\frac{y - y_0}{x - x_0} \right) \right] \\ &\quad \times \exp \left[-iq \tan^{-1} \left(\frac{y - y_0}{x + x_0} \right) \right], \quad (22) \end{aligned}$$

where $(\pm x_0, y_0)$ are the location of the vortex and antivortex of the vortex dipole, and q is the charge of the

imprinted vortices. Since singly charged vortices are energetically favorable compared to the multiply charged vortices [51], we shall consider only singly charged vortices ($|q|=1$).

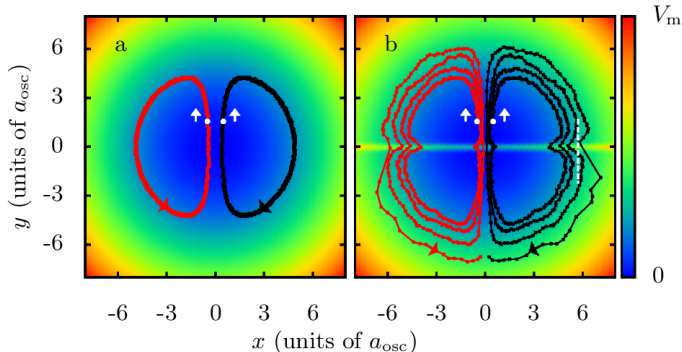


FIG. 1. (Color online) Motion of a vortex dipole in an external trapping potential. (a) shows the trajectory of the vortex dipole in the absence of the barrier potential, (b) shows the trajectory of the vortex dipole in the presence of the barrier potential. The initial position ($\mp 0.5, 1.5$) and direction of the motion of the vortex and antivortex are shown by white dots and arrows, respectively. The red (black) lines show the trajectories of vortex (antivortex) where direction of the movement of the vortices is shown by the arrows. The straight dashed white line in (b) shows the decrease in the curvature of equipotential lines when the antivortex crosses the barrier potential. The maxima of external trapping potential V_m is $128 \hbar\omega_{\perp}$.

To study the dynamics, we consider the converged solution from the imaginary time propagation as the initial state and propagate it in real time. For the axisymmetric trap considered here, we observe the acceleration of vortices due to their mutual velocity fields which induces emission of acoustic waves. During the dynamical evolution, as the vortex-antivortex pair approaches the origin their separation decreases and appears to coalesce but do not annihilate [21]. After wards, they separate and continue to move. Thus, the vortex dipole exhibits periodic orbital motion and the position of the vortices at different times during three orbital cycles are shown in Fig. 1(a) and Fig. 2, respectively. We observe that the vortex dipole survives for many seconds without annihilation which was reported in our previous work [21] and is consistent with the experimental results [16].

A. Effect of barrier potential

To examine the interaction of a vortex dipole with barrier, we introduce repulsive Gaussian barrier potential V_{bar} along the x -direction. In the present study, we vary V_0 but set $w = 1.0 \mu\text{m}$. The trajectories of the vortex and antivortex in the presence of the barrier is shown in Fig. 1(b) for the case of $V_0 = 15$ (in units of $\hbar\omega_{\perp}$). Furthermore, the temporal variation of v_{2x} , the x -component of

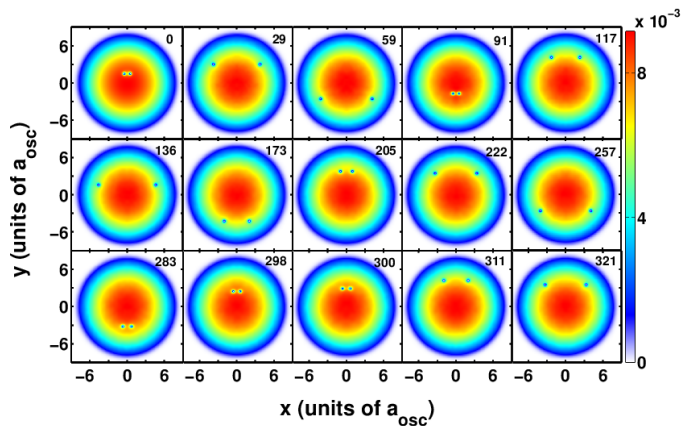


FIG. 2. (Color online) Condensate density profiles showing the dynamics of a vortex dipole in a harmonically trapped BEC (in the absence of the barrier potential) obtained using numerical integration of 2D GPE. The vortex and antivortex are imprinted at $(x_0 = \mp 0.5, y_0 = 1.5)$. The vortex dipole completes its first, second and third orbit at around 96 ms, 187 ms, and 292 ms respectively. The time (in units of ms) is shown at the top right corner of each image. Density is measured in units of a_{osc}^{-2} and is normalized to unity.

the antivortex velocity, with and without the barrier are shown as black and red curves, respectively, in Fig. 3(a). As expected, without the barrier, v_{2x} has periodic variation as the vortex precess in a semicircular trajectory and the first half-sinusoid in Fig. 3(a) represents v_{2x} for the $y > 0$ part of the first orbit. Similarly, the second half-sinusoid correspond to the v_{2x} for the $y < 0$ part. The zero of v_{2x} occurs when the position of the antivortex has $y \sim 0$, which is consistent with the expression of \mathbf{v}_2 in Eq. (8).

The temporal variation of v_{2y} , on the other hand, exhibits a minor difference. One orbit comprises of two slightly different half-sinusoids, rounded and sharp maxima. These correspond to the relatively curved and straight parts of the trajectory, respectively. As the dissipation is negligible, the antivortex continues in the semicircular orbit and this is reflected in the periodic patterns of v_{2x} and v_{2y} . This is also clearly discernible from Fig. 1(a), which is an overlap of the snapshots of the vortex and antivortex positions over four orbits. We also calculate the velocity profile of the antivortex analytically using Eq. (8). We find that our analytical results are in good agreement with the numerical calculations shown in Fig. (3).

Introducing the barrier potential brings out a marked change in v_{2x} when the antivortex position has $|y| \leq w$. As the antivortex enters this region $y \in [w, 0]$, it experiences a sharp deceleration. The velocity then becomes zero at $y = 0$, which is identified based on the numerical results. For the $y \approx 0$ domain, the variation of v_{2x} is consistent with Eq. (9), where it is shown that $v_{2x} \propto y$. Again, for $y \in [0, -w]$ the antivortex experiences acceleration till it leaves the barrier region. As evident from

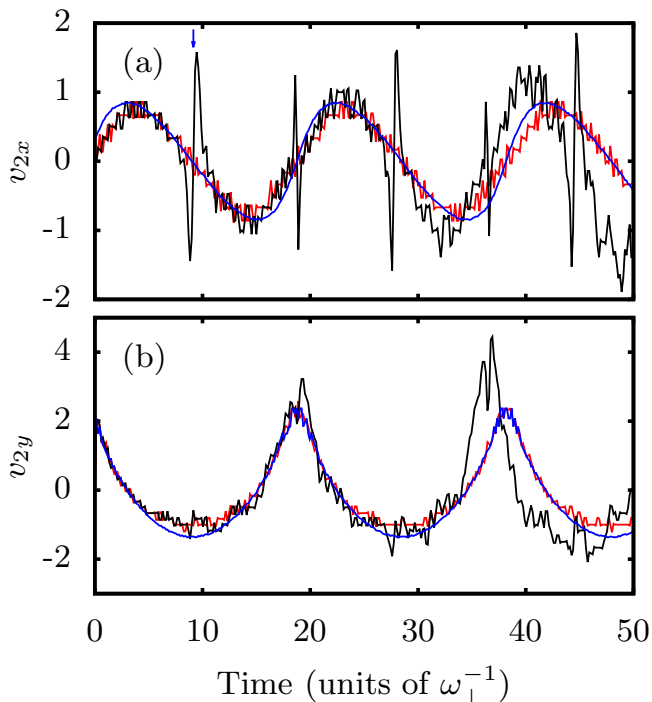


FIG. 3. (Color online) The velocity components of the antivortex with (without) the barrier potential. (a) Black (red) curve represents the temporal variation of v_{2x} with (without) the barrier potential. The blue arrow indicates the instant of time when v_{2x} is zero. (b) Black (red) curve represents temporal variation in v_{2y} . Blue curve shown is the analytical result obtained from Eq. (8). Here the velocity components are expressed in units of $a_{\text{osc}}\omega_{\perp}$.

the Fig. 3, the antivortex experiences a large change in the velocity when it encounters the barrier and dissipates energy through acoustic radiation. This causes an increase in the radius of the semi-circular orbit and a corresponding increase in time period of the orbit. This is also evident from Fig. 1(b), which shows both the vortex and antivortex spiral away from the initial orbits due to energy dissipation of the vortex dipole through the acoustic radiation. As an example, the change in the radius of one of the orbits of the antivortex before and after passing through the barrier is indicated with a dashed white line in Fig. 1(b).

During the first orbit, unlike v_{2x} , there is little or no effect to the v_{2y} in the presence of the barrier. But, there are changes in v_{2y} during the later orbits. These are noticeable in Fig. 3, where there is a periodic variation in v_{2x} and v_{2y} .

In presence of the barrier, as discussed earlier, there is a correction to the TF density profile within the neighborhood of the barrier potential. To verify the analytic expression derived earlier, we compare it with the results from numerical solution of the GPE. In Fig. 4, we show the plots of the correction to TF-approximation obtained from the numerical solution of GPE and estimated using the analytic expression in Eq. (15). It is evident from the

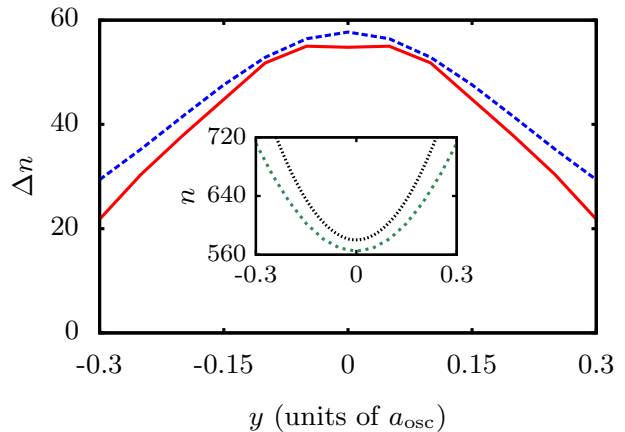


FIG. 4. (Color online) The correction to condensate density along y -direction near the barrier for the quasi 2D BEC. The red-solid line shows the correction to density calculated numerically by subtracting TF solution from the actual GPE solution. The blue-dashed line shows the correction to TF approximation near the repulsive barrier which has been calculated analytically from Eq. (15). Inset: The green-dashed and black-dotted lines are the density profile of the condensate along y -direction within the barrier region calculated using numerical computation and analytically from Eq. (13), respectively. The density is normalized to the total number of atoms N in the condensate.

figure that the results from the analytic expression is in good agreement with the numerical result, at the center the analytical result is approximately 5% higher than the numerical result.

It should be emphasized here that the dynamics of a vortex-antivortex pair also depends on the initial distance between the constituent vortices as reported in Crasovan *et. al* [52]. Depending on the initial position and separation, but with the same set of parameters, a range of scenarios are possible. In the presence of the barrier, beyond a critical separation ($\sim 1.6a_{\text{osc}}$), the vortex dipole does not cross the barrier and move in a closed orbit on one side of the barrier. For lower values of vortex-antivortex separation the vortex dipole crosses the barrier and dissipates kinetic energy during each crossing. In our present work we examine vortex-barrier interaction for a fixed value of vortex-antivortex separation, and thus studying the aforementioned dynamics for varying vortex-antivortex distance will be investigated in detail in our future works.

B. Energetics

To estimate the energy transferred to the acoustic field by the vortex, consider the energy of a vortex located at a distance b from the z -axis in quasi-2D geometry [51]

$$E \simeq E_0 \left(1 - \frac{b^2}{R_{\perp}^2}\right)^{3/2}, \quad (23)$$

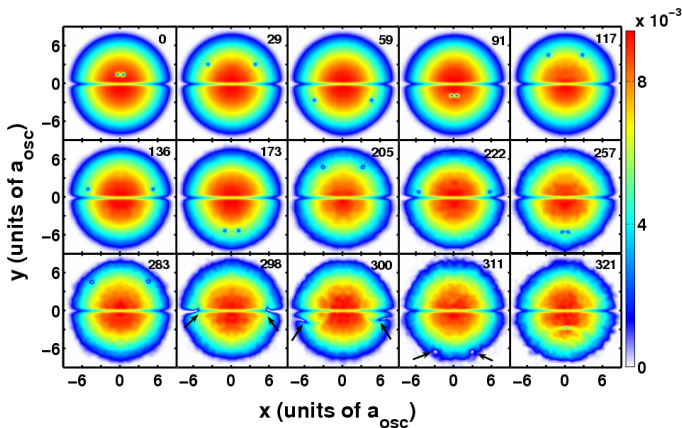


FIG. 5. (Color online) Condensate density profiles showing the dynamics of a vortex dipole in a harmonically trapped BEC in the presence of the barrier potential. The vortex-antivortex pair annihilates at $t = 320$ ms. Density is measured in units of a_{osc}^{-2} and is normalized to unity. The vortex-antivortex pair follows the trajectories given in the Fig. 1(b). In the bottom panels the vortex and antivortex are indicated by the black arrows.

where $E_0 = [4\pi\hbar^2 n(0,0)Z/(3m)] \ln(R_{\perp}/\xi)$ with Z as the semi-axis along the z -axis and $n(0,0)$ is the density at the origin. The above relation is applicable when $Z \gg \xi$ and holds true for the parameters we have considered. Based on the above expression, the energy radiated by a vortex when the radius of the orbit is increased from b to $b + \Delta b$ is $\Delta E \simeq 3(E_0 b/R_{\perp}^3) \sqrt{R_{\perp}^2 - b^2} \Delta b$. From this relation, the energy released by the vortex when it crosses the barrier potential in the orbit marked by the dashed line in Fig. 1(b) is $2.1 \times 10^{-3} \hbar\omega_{\perp}$ and corresponding change in the orbital radius Δb is $0.5a_{\text{osc}}$. It is to be noted that the value of Δb increases and during the fourth orbit the vortex dipole annihilates. For the present case, $V_0 = 15\hbar\omega_{\perp}$, the condensate profile at selected time steps are shown in Fig. 5. The annihilation of the vortex dipole during the fourth orbital motion is clearly discernible in Fig. 5 for the snapshot corresponding to 321 ms. Considering that the radius b before the annihilation is $7.08a_{\text{osc}}$, and vortex and antivortex carry same kinetic energy, the energy released during annihilation is $5.21 \times 10^{-3} \hbar\omega_{\perp}$.

To study the effect of the barrier on the dynamics of the vortex dipole, we further increase V_0 to values higher than $15\hbar\omega_{\perp}$ and observe the temporal evolution of the system. At low values, $V_0 < 25\hbar\omega_{\perp}$, the vortex dipole crosses the barrier. However, the vortex dipole dissipates energy during the crossing and at a later stage, the vortex dipole self annihilates. At higher V_0 , the annihilation of the dipole occurs in even less time. But, when V_0 is larger than a critical value ($25\hbar\omega_{\perp}$), the vortex dipole does not cross the barrier and bounces from the barrier.

To analyze the energetics associated with the vortex dipole annihilation, we examine the contribution from various component to the total energy. The total energy

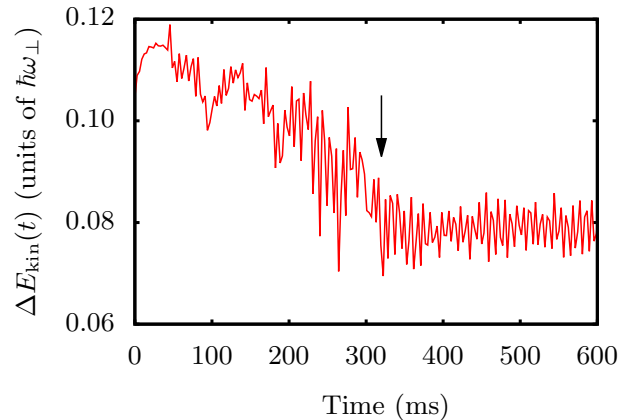


FIG. 6. Decay of $\Delta E_{\text{kin}}(t)$ due to interaction of vortex dipole with barrier in the harmonically trapped quasi-2D BEC. The annihilation event at 320 ms is indicated by an arrow.

of the condensate E_{tot} , in general, is the sum of kinetic energy E_{kin} , interaction energy E_{int} , quantum pressure energy E_{q} and external trapping potential energy E_{ext} . So, we can write

$$E_{\text{tot}} = E_{\text{kin}} + E_{\text{int}} + E_{\text{q}} + E_{\text{ext}}, \quad (24)$$

where

$$E_{\text{kin}}(t) = \frac{1}{2} \int [\sqrt{n(x,y,t)} \mathbf{v}(x,y,t)]^2 dx dy, \quad (25a)$$

$$E_{\text{int}}(t) = \int g[n(x,y,t)]^2 dx dy, \quad (25b)$$

$$E_{\text{q}}(t) = \frac{1}{2} \int [\nabla \sqrt{n(x,y,t)}]^2 dx dy, \quad (25c)$$

$$E_{\text{ext}}(t) = \int n(x,y,t) V_{\text{ext}} dx dy, \quad (25d)$$

where the velocity $\mathbf{v} = \nabla \phi(x,y,t)$. Here, all energies are in scaled units, as defined earlier. To examine the kinetic energy of the vortex dipole dissipated, define

$$\Delta E_{\text{kin}}(t) = E_{\text{kin}}^{\text{vd}}(t) - E_{\text{kin}}^0(t), \quad (26)$$

where $E_{\text{kin}}^{\text{vd}}$ and E_{kin}^0 are the kinetic energies of the condensate with and without the vortex dipole, respectively. In the case of $E_{\text{kin}}^{\text{vd}}(t)$, it can further be decomposed into a component arising from the kinetic energy (KE) of the vortex dipole and a part due to the acoustic field. The temporal variation of $\Delta E_{\text{kin}}(t)$ provides a measure of the kinetic energy of the vortex dipole transformed into acoustic energy and is shown in Fig. 6. After the vortex dipole undergoes annihilation, marked by an arrow in Fig. 6 at $t \sim 320$ ms, a part of the kinetic energy gets transformed into acoustic radiation energy and the remaining into the interaction energy. So, for $t > 320$ ms the mean value of $\Delta E_{\text{kin}}(t)$ after the annihilation is associated with energy of the acoustic field in the condensate. In this time domain, the $\Delta E_{\text{kin}}(t)$ shows rapid variations but are devoid of low-frequency oscillations associated with the KE of vortex dipole.

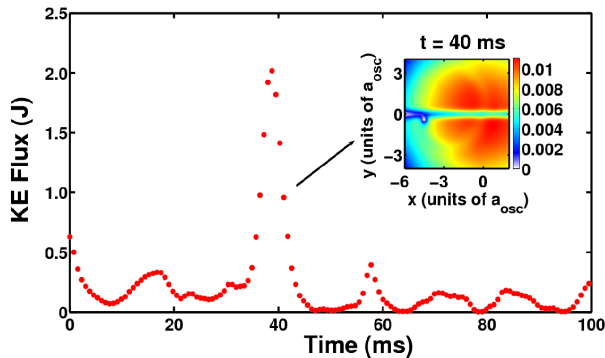


FIG. 7. (Color online) The power radiated by a single vortex is shown as a function of time as it passes through a repulsive Gaussian barrier. The inset figure shows the density variation and acoustic wave, which is emitted due to vortex-barrier interaction at $t \approx 40$ ms. At $t = 0$, the vortex is imprinted at $x_0 = 0$, $y_0 = 3.5$.

We numerically calculate the kinetic energy lost by the vortex near static barrier due to radiation. In order to calculate the KE flux we numerically solve Eq. (19) in the far-field approximation. During each crossing of the barrier, the vortex emits acoustic radiation that significantly perturbs the vortex trajectory. The power radiated due to vortex-barrier interaction is shown in Fig. 7, where a large decay in energy of the vortex dipole is discernible at 40 ms. In addition, the vortex also radiates, much lower flux, in the bulk of the condensate due to the acceleration arising from the precession. This is evident from the small peaks in the KE flux around 40 ms. Due to the radial dependence of the acoustic velocity, after emission the acoustic waves acquire bow-shaped geometry. At a later time the acoustic waves reflect from the edge of the condensate and interact with vortex. In the limit of large V_0 the vortex reflects back from the barrier and eventually, due to energy loss it precess outwards and is lost from the condensate bulk. Apart from radiation induced energy dissipation, the broken rotational

symmetry of the system also affects the life time of the vortex in the condensate [30].

IV. CONCLUSIONS

In summary, we studied the effects on a single vortex or a vortex dipole of a static Gaussian barrier within a harmonically trapped BEC. We not only examined the dynamics of a vortex dipole, but also analytically calculated the velocity of the constituent vortices in this setting. The analytical results are compared with the numerical solutions and we find that these are in good agreement. Unlike in the absence of a barrier, we have further demonstrated that the presence of a barrier modifies the trajectory of the vortex dipole. Furthermore we have also shown that the density anisotropy introduced by the barrier enhances the possibility of annihilation events of vortex dipole in atomic BECs through acoustic radiation.

This work opens up the possibility of future investigations on the topic of vortex-barrier interactions. Among the many interesting prospects that can be considered are studying the effects of different kinds of barrier on the vortex dynamics. The vortex-antivortex separation can also be tuned to study a large number of possible scenarios. Even role of finite temperature on vortex-barrier interaction is a possible natural extension of the present work.

ACKNOWLEDGMENTS

We thank S. Gautam and S. Chattopadhyay for very useful discussions. The results presented in the paper are based on the computations using the 3TFLOPs HPC Cluster at Physical Research Laboratory, Ahmedabad, India. We also thank the anonymous referees for their thorough review and valuable comments, which contributed to improving the quality of the manuscript.

-
- [1] L. M. Pismen, *Vortices in Nonlinear Fields* (Clarendon, Oxford, 1999)
 - [2] M. Kobayashi and M. Tsubota, *Phys. Rev. A* **76**, 045603 (2007)
 - [3] E. A. L. Henn, J. A. Seman, G. Roati, K. M. F. Magalhães, and V. S. Bagnato, *Phys. Rev. Lett.* **103**, 045301 (2009)
 - [4] M. H. Anderson, J. R. Ensher, M. R. Matthews, C. E. Wieman, and E. A. Cornell, *Science* **269**, 198 (1995)
 - [5] K. B. Davis, M. O. Mewes, M. R. Andrews, N. J. van Druten, D. S. Durfee, D. M. Kurn, and W. Ketterle, *Phys. Rev. Lett.* **75**, 3969 (1995)
 - [6] C. C. Bradley, C. A. Sackett, J. J. Tollett, and R. G. Hulet, *Phys. Rev. Lett.* **75**, 1687 (1995)
 - [7] R. P. Feynman, in *Progress in Low Temperature Physics*, Vol. 1, edited by C. J. Gorter (North-Holland, Amsterdam, 1955)
 - [8] L. Onsager, *Nuovo Cimento* **6**, Suppl. 2, 249 (1949)
 - [9] M. R. Matthews, B. P. Anderson, P. C. Haljan, D. S. Hall, C. E. Wieman, and E. A. Cornell, *Phys. Rev. Lett.* **83**, 2498 (1999)
 - [10] K. W. Madison, F. Chevy, W. Wohlleben, and J. Dalibard, *Phys. Rev. Lett.* **84**, 806 (2000)
 - [11] J. R. Abo-Shaeer, C. Raman, J. M. Vogels, and W. Ketterle, *Science* **292**, 476 (2001)
 - [12] G. Andrejczyk, M. Brewczyk, L. Dobrek, M. Gajda, and M. Lewenstein, *Phys. Rev. A* **64**, 043601 (2001)
 - [13] A. E. Leanhardt, A. Görlitz, A. P. Chikkatur, D. Kielpinski, Y. Shin, D. E. Pritchard, and W. Ketterle, *Phys. Rev. Lett.* **89**, 190403 (2002)

- [14] D. V. Freilich, D. M. Bianchi, A. M. Kaufman, T. K. Langin, and D. S. Hall, *Science* **329**, 1182 (2010)
- [15] D. R. Scherer, C. N. Weiler, T. W. Neely, and B. P. Anderson, *Phys. Rev. Lett.* **98**, 110402 (2007)
- [16] T. W. Neely, E. C. Samson, A. S. Bradley, M. J. Davis, and B. P. Anderson, *Phys. Rev. Lett.* **104**, 160401 (2010)
- [17] J. Brand and W. P. Reinhardt, *Phys. Rev. A* **65**, 043612 (2002)
- [18] L. Pitaevskii and S. Stringari, *Bose-Einstein Condensation* (Clarendon, Oxford, 2003)
- [19] A. L. Fetter and A. A. Svidzinsky, *J. Phys.: Condens. Matter* **13**, R135 (2001)
- [20] T. Aioi, T. Kadokura, T. Kishimoto, and H. Saito, *Phys. Rev. X* **1**, 021003 (2011)
- [21] S. Prabhakar, R. P. Singh, S. Gautam, and D. Angom, *J. Phys. B* **46**, 125302 (2013)
- [22] S. Gautam, A. Roy, and S. Mukerjee, *Phys. Rev. A* **89**, 013612 (2014)
- [23] K. Fujimoto and M. Tsubota, *Phys. Rev. A* **83**, 053609 (2011)
- [24] P. Mason and N. G. Berloff, *Phys. Rev. A* **77**, 032107 (2008)
- [25] V. Pietilä, M. Möttönen, T. Isoshima, J. A. M. Huh-tamäki, and S. M. M. Virtanen, *Phys. Rev. A* **74**, 023603 (2006)
- [26] S. Gautam, P. Muruganandam, and D. Angom, *J. Phys. B* **45**, 055303 (2012)
- [27] S. Gautam, P. Muruganandam, and D. Angom, *Phys. Lett. A* **377**, 378 (2013)
- [28] T. Aioi, T. Kadokura, and H. Saito, *Phys. Rev. A* **85**, 023618 (2012)
- [29] W. F. Vinen, *Phys. Rev. B* **64**, 134520 (2001)
- [30] E. Lundh and P. Ao, *Phys. Rev. A* **61**, 063612 (2000)
- [31] N. G. Parker, N. P. Proukakis, C. F. Barenghi, and C. S. Adams, *Phys. Rev. Lett.* **92**, 160403 (2004)
- [32] C. F. Barenghi, N. G. Parker, N. P. Proukakis, and C. S. Adams, *J. Low Temp. Phys.* **138**, 629 (2005)
- [33] N. G. Parker, A. J. Allen, C. F. Barenghi, and N. P. Proukakis, *Phys. Rev. A* **86**, 013631 (2012)
- [34] B. Y. Rubinstein and L. M. Pismen, *Physica D* **78**, 1 (1994)
- [35] A. A. Svidzinsky and A. L. Fetter, *Phys. Rev. A* **62**, 063617 (2000)
- [36] A. Nayfeh, *Perturbation Methods* (Wiley-VCH, Weinheim, 2008)
- [37] L. Koens and A. M. Martin, *Phys. Rev. A* **86**, 013605 (2012)
- [38] G. Wolf, in *NIST Handbook of Mathematical Functions*, edited by F. W. J. Olver, D. W. Lozier, R. F. Boisvert, and C. W. Clark (Cambridge University Press, 2010)
- [39] W. Li, M. Haque, and S. Komineas, *Phys. Rev. A* **77**, 053610 (2008)
- [40] E. Lundh, C. J. Pethick, and H. Smith, *Phys. Rev. A* **55**, 2126 (1997)
- [41] F. Dalfovo, L. Pitaevskii, and S. Stringari, *Phys. Rev. A* **54**, 4213 (1996)
- [42] A. L. Fetter and D. L. Feder, *Phys. Rev. A* **58**, 3185 (1998)
- [43] D. P. Arovos and J. Freire, *Phys. Rev. B* **55**, 1068 (1997)
- [44] T. Kambe, *J. Fluid Mech.* **173**, 643 (1986)
- [45] C. Nore, M. Abid, and M. E. Brachet, *Phys. Fluids* **9**, 2644 (1997)
- [46] G. Krstulovic, M. Brachet, and E. Tirapegui, *Phys. Rev. E* **78**, 026601 (2008)
- [47] D. M. Jezek, P. Capuzzi, M. Guilleumas, and R. Mayol, *Phys. Rev. A* **78**, 053616 (2008)
- [48] D. M. Jezek and H. M. Cataldo, *Phys. Rev. A* **77**, 043602 (2008)
- [49] P. Muruganandam and S. K. Adhikari, *Comp. Phys. Comm.* **180**, 1888 (2009)
- [50] L. Dobrek, M. Gajda, M. Lewenstein, K. Sengstock, G. Birkl, and W. Ertmer, *Phys. Rev. A* **60**, R3381 (1999)
- [51] C. Pethick and H. Smith, *Bose-Einstein Condensation in Dilute Gases* (Cambridge University Press, 2008)
- [52] L.-C. Crasovan, V. Vekslerchik, V. M. Pérez-García, J. P. Torres, D. Mihalache, and L. Torner, *Phys. Rev. A* **68**, 063609 (2003)